TOPOLOGY DESIGN OF THERMOMECHANICAL ACTUATORS

S.M. GIUSTI, Z. MRÓZ, A.A. NOVOTNY, AND J. SOKOŁOWSKI

ABSTRACT. The paper deals with topology design of thermomechanical actuators. The goal of shape optimization is to maximize the output displacement in a given direction on the boundary of the elastic body, which is submitted to a thermal excitation that induces a dilatation/contraction of the thermomechanical device. The optimal structure is identified by an elastic material distribution, while a very compliant (weak) material is used to mimic voids. The mathematical model of an actuator takes the form of a semi-coupled system of partial differential equations. The boundary value problem includes two components, the Navier equation for linear elasticity coupled with the Poisson equation for steady-state heat conduction. The mechanical coupling is the thermal stress induced by the temperature field. Given the integral shape functional, we evaluate its topological derivative with respect to the nucleation of a small circular inclusion with the thermomechanical properties governed by two contrast parameters. The obtained topological derivative is employed to generate a steepest descent direction within the level set numerical procedure of topology optimization in a fixed geometrical domain. Finally, several finite element-based examples for the topology design of thermomechanical actuators are presented.

1. INTRODUCTION

In this paper the topology design of thermomechanical actuators is considered in two spatial dimensions for a linear multiphysics model (Sigmund, 1997; Kikuchi et al., 1998; Li et al., 2004; Rubio et al., 2010). The boundary value problem of elliptic type is given by the linearized elasticity coupled with the steady-state heat conduction problem. The reference configuration of the structure is an open and bounded domain $\Omega \subset \mathbb{R}^2$, with Lipschitz boundary denoted as $\partial\Omega$. The topology is identified through the distribution of elastic material within Ω and the voids are mimicked by a very compliant (weak) material. Therefore, topological changes of the reference domain are defined by the nucleation of inclusions with the thermomechanical properties governed by two contrast parameters. In order to determine the best distribution of elastic material the method of topological derivatives (Sokołowski and Żochowski, 1999) is employed. The shape variations of boundaries and interfaces between elastic and compliant materials are also allowed during the shape-topological optimization. The displacement field in the structure is determined within the framework of linearized elasticity with thermally induced stresses. The temperature field satisfies the steady-state heat conduction equation. The state variables include the displacement field u and the temperature field θ. The shape functional $\Omega \mapsto J(\Omega)$ to be minimized is given by the line integral of $g = -u \cdot e$ on the portion $\Gamma^\star$ of the boundary $\partial\Omega$. Hence, the output displacement u on $\Gamma^\star$ is maximized in a given direction e. For the sake of motivation, let us consider an example which shows that the optimum design of the simple thermomechanical structure does not follow from an intuitive reasoning, namely thermal distortion design of switching device.

1.1. **Simple example of a bar structure.** Consider two bars AP and BP of the length $l = \frac{L}{2}$ and with the joint at P, see Fig. 1. The bars are fixed at the points A and B. The length AB of the isosceles triangle APB is $2a$, while a is the design variable. We set $2l = L = const$, where $a = l\cos\beta = \frac{L}{2}\cos\beta$ is varying, and $h = l\sin\beta = \frac{L}{2}\sin\beta$. We want to specify the configuration of two bars for which $\frac{\Delta h}{L}$ is maximum within the admissible configurations of $0 < \beta \leq \frac{\pi}{2}$. The structure is uniformly heated up to the temperature θ, which produces a thermal distortion strain given by $\epsilon_\theta = \alpha\theta$, where α is the thermal expansion coefficient. It is easy to derive the expression for the non-dimensional displacement δ, namely

$$\delta := \frac{\Delta h}{L} = \frac{1}{2}\left[\sqrt{\sin^2\beta + 2\alpha\theta + \alpha^2\theta^2} - \sin\beta\right]$$

and evaluate its derivatives

$$S_\beta := \frac{\partial}{\partial\beta}\left(\frac{\Delta h}{L}\right) = -\frac{\delta\cos\beta}{2\delta + \sin\beta} < 0$$

and

$$S_\theta := \frac{\partial}{\partial\theta}\left(\frac{\Delta h}{L}\right) = \frac{1}{2}\left(\frac{\alpha + \alpha^2\theta}{2\delta + \sin\beta}\right).$$

Since the sensitivity derivative S_β in function of the angle β, decreasing in the interval $(0, \frac{\pi}{2}]$, thus the

maximum is located at $\beta = \beta_0$, where $0 < \beta_0 \ll 1$ is a small value of β inducing an upward displacement. In particular, $\beta = \frac{\pi}{2}$ is actually the worst case. It is interesting to note that the maximal value of Δh due to combined rotation and extensionof bars at $\beta = 0$. This example provides the insight into the principle of optimal design, where the thermal strain induces large rotation of material elements
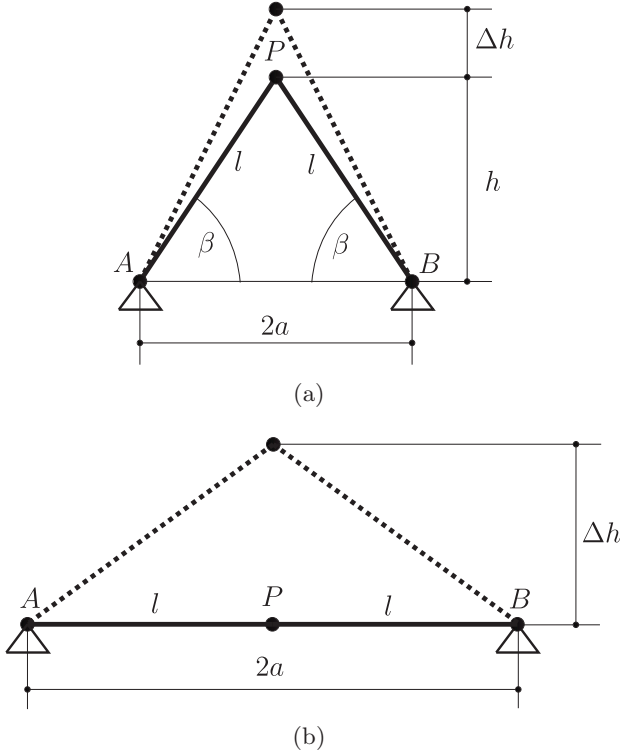

FIGURE 1. Truss subject to thermal effects: (a) initial guess and (b) optimal layout.

1.2. **Topological derivative for inclusions.** Without loss of generality the topological sensitivity analysis of the given shape functional $\Omega \mapsto J(\Omega)$ can be performed for a single circular inclusion $\varepsilon \mapsto B_\varepsilon(\widehat{x})$. Here $B_\varepsilon(\widehat{x}) = \{\|x - \widehat{x}\| < \varepsilon\}$ is a ball with the fixed centre $\widehat{x} \in \Omega$, so the location of the ball in the reference domain is uniquely determined by its centre. The insertion of inclusion B_ε into the reference domain results in the local perturbation of material properties of the reference domain and it makes the shape functional dependent on the small parameter $\varepsilon \to 0$. In particular, the topologically perturbed counterpart of the shape functional $\varepsilon \mapsto B_\varepsilon \mapsto J_\varepsilon(\Omega)$ is given by the line integral of $g_\varepsilon = -u_\varepsilon \cdot e$ on the portion $\Gamma^\star$ of the boundary $\partial\Omega$. Hence, the output displacement u_ε depends on the inclusion B_ε with the centre $\widehat{x}$ and such that $\varepsilon \to 0$. The dependence of

the shape functional results from the state equation, where the small inclusion makes the coefficients of Navier and Poisson equations dependent on the characteristic function of $B_\varepsilon(\widehat{x})$, with $\varepsilon \to 0$ used for the asymptotic analysis. Thus, the interesting question from the point of view of shape-topological optimization is the existence of the asymptotic expansion at $\varepsilon = 0^+$ for the function $\varepsilon \mapsto J_\varepsilon(\Omega)$. Such an asymptotic expansion is established in the paper. The first term of obtained asymptotic expansion is the so-called topological derivative of the shape functional. The topological derivative depends on the solutions u and θ, as well as on their corresponding adjoint states p and φ, all of them evaluated at the centre $\widehat{x}$. It also depends on the material parameters of the background as well as on γ^M and γ^T, which are called the contrast for mechanical and thermal material properties of B_ε, respectively. In this way an optimal location of a small inclusion and its properties can be determined in order to minimize the shape functional associated with the model. The topological derivative of the elastic energy associated with such a thermomechanical model has been derived by Giusti et al. (2013). However, to the best of our knowledge the topological sensitivity analysis of a shape functional specially designed for topology optimization purposes of thermomechanical actuators cannot be found in the literature. Therefore, we derive with all details the topological asymptotic expansion of the adopted shape functional and perform a complete mathematical justification for the obtained formulas.

The paper is organized as follows. In Section 2 the topological derivative concept is introduced in the framework of asymptotic analysis of a singulary perturbed domain. The semi-coupled system modeling the thermomechanical actuator as well as the adopted shape functional are presented in Section 3. The associated topological asymptotic expansion is rigorously derived in Section 4. In Section 5 some numerical experiments of topology optimization of thermomechanical actuators are presented. Finally, the concluding remarks and perspectives are given in Section 6.

2. Topological Derivative Concept

The mathematical model of the actuator is given by coupled linear equations of elliptic type. Hence, it can be shown by the standard procedure of the speed method (Sokołowski and Zolésio, 1992) that the elliptic boundary value problem under consideration is

well posed from the point of view of shape optimization. In particular, it means that by the elliptic regularity of the weak solutions to the model, the existence of the shape and material derivatives is ensured. This fact implies the existence of the shape gradient for the boundary shape functional. Therefore, the classical shape optimization method by boundary variations can be applied for numerical solution of the shape optimization problem. We are interested, however, in modern approaches to shape-topological optimization, i.e., we want to admit a broader family of admissible domains obtained by non smooth perturbations of regular domains. In other words, we perform the asymptotic analysis of solutions to the state equation in the singularly perturbed geometrical domains. The non smooth domain perturbations can be analyzed only in the framework of asymptotic analysis (Novotny and Sokołowski, 2013) because such perturbations cannot be described by bilipschitzian mappings of the speed method. The singular perturbations include the insertion of holes or cavities into the reference domain. It is known (Novotny and Sokołowski, 2013) that the holes or cavities can be considered as the limit case of inclusions for the limit passage of the so-called contrast parameters. For numerical solution of optimum design problems it is useful to insert inclusions made of a different material characterized by two contrast parameters for elastic and thermal properties.

The starting point of the numerical procedure for structural optimum design is numerical evaluation of the topological derivative. Actually, the topological derivative formula is obtained at the continuous level. In order to use this information for the purposes of identifying local minima or maxima in a numerical optimization procedure we need the discrete values of the topological derivative. The precision of numerical evaluation of topological derivatives should be sufficient for such an identification procedure. In the case of minimization problems, we select the negative part of the level-set function associated with the topological derivative evaluated in the reference domain. Therefore, we are looking for the local minima of the topological derivative for one isolated circular inclusion $B_\varepsilon(\widehat{x})$, for all $\widehat{x} \in \Omega$. Let us recall that the topological derivative for one circular inclusion $B_\varepsilon \mapsto J_\varepsilon(\Omega)$ is a function $\widehat{x} \mapsto \mathcal{T}(\widehat{x})$ defined in Ω such that the following asymptotic expansion holds for $\varepsilon \to 0$,

$$J_\varepsilon(\Omega) = J(\Omega) + f(\varepsilon)\mathcal{T}(\widehat{x}) + o(f(\varepsilon)). \qquad (2.1)$$

The function $f(\varepsilon)$, such that $f(\varepsilon) \to 0^+$ with $\varepsilon \to 0^+$, can be specified from the asymptotic analysis with respect to the small parameter $\varepsilon \to 0$.

The insertion of one inclusion results in perturbations of the coefficients of the elliptic operators. For one inclusion, we perform the sensitivity analysis of the perturbed coupled equations with respect to the small parameter $\varepsilon \to 0$. Such an analysis gives rise for $\varepsilon > 0$ of the shape gradient of the specific shape functional $\varepsilon \mapsto J_\varepsilon(\Omega)$. By the limit transition $\varepsilon \to 0^+$ the topological derivative of the functional is obtained as a function of the point $\widehat{x} \in \Omega$. This means that for fixed ε there are known two expansions of the cost $\varepsilon \mapsto j(\varepsilon) := J_\varepsilon(\Omega)$, with respect to the small parameters $\delta \to 0$ and $\varepsilon \to 0^+$, respectively

- for $\varepsilon > 0$,

$$j(\varepsilon + \delta) = j(\varepsilon) + \delta j'(\varepsilon) + O(\delta^2), \qquad (2.2)$$

- for $\varepsilon = 0^+$,

$$j(\varepsilon) = j(0) + f(\varepsilon)\mathcal{T}(\widehat{x}) + o(f(\varepsilon)). \qquad (2.3)$$

By $j'(\varepsilon)$ is denoted the classical shape derivative of the cost functional $J_\varepsilon(\Omega)$ with respect to the shape perturbations of the boundary of inclusion $B_\varepsilon(\widehat{x})$. The second formula of asymptotic type is established for the radius $\varepsilon = 0^+$ of the inclusion. Therefore, we are going to determine the unknown function

$$\widehat{x} \mapsto \mathcal{T}(\widehat{x}), \qquad (2.4)$$

by the method of asymptotic analysis. We recall (Żochowski, 1988) that there is a relation between the two formulas (2.2) and (2.3), namely:

$$\mathcal{T}(\widehat{x}) = \lim_{\varepsilon \to 0^+} \frac{j'(\varepsilon)}{f'(\varepsilon)}. \qquad (2.5)$$

In addition, we point out that the topological derivative, whenever it does exist, can be considered as an extension of the shape derivative of the cost functional, since the topological derivative can be evaluated in the domain Ω as well as on its boundary $\partial\Omega$. See for instance applications of the topological derivative concept in the context of inverse problems (Hintermüller et al., 2012), structural topology optimization (Mróz and Bojczuk, 2012), image processing (Hintermüller and Laurain, 2009), multi-scale material design (Amstutz et al., 2010) and mechanical modeling including damage (Allaire et al., 2011) and fracture (Van Goethem and Novotny, 2010) evolution phenomena.

3. Problem Formulation

Let us now introduce the thermomechanical semi-coupled model. The displacement field is determined within linear elasticity with thermally induced stresses for isotropic materials. The temperature field is described by the steady-state heat conduction

4

equation. The state variables include the displacement field and the temperature field.

3.1. **Unperturbed Problem.** The shape functional to be minimized is given by a line integral

$$j(0) = J(\Omega) = \mathcal{J}_\Omega(u) := -\int_{\Gamma^\star} e \cdot u, \qquad (3.1)$$

where $\Gamma^\star$ is a part of the boundary $\partial\Omega$ and the structural displacement u has to be maximized in a given unity direction e.

The vector function u solves the following thermo-mechanical equilibrium problem:

$$u \in \mathcal{V}(\Omega) : \int_\Omega S(u) \cdot (\nabla v)^s = 0 \quad \forall v \in \mathcal{V}(\Omega). \quad (3.2)$$

Some terms in the above equation require explanation. The Cauchy stress tensor $S(u)$ is given by

$$S(u) = \mathbb{C}((\nabla u)^s - \alpha\theta\,\mathrm{I}) = \sigma(u) - \beta\theta\,\mathrm{I}, \qquad (3.3)$$

where $(\nabla u)^s$ is used to denote the symmetric part of the gradient of the displacement field u, i.e.

$$(\nabla u)^s := \frac{1}{2}(\nabla u + (\nabla u)^\top). \qquad (3.4)$$

In addition, $\mathbb{C}$ denotes the fourth-order elasticity tensor, which for isotropic materials is given by

$$\mathbb{C} = 2\mu\mathbb{I} + \lambda(\mathrm{I} \otimes \mathrm{I}), \qquad (3.5)$$

where μ and λ are the Lamé coefficients. The second order tensor $\sigma(u)$ is related to the total displacement field by the Hooke's law

$$\sigma(u) := \mathbb{C}(\nabla u)^s, \qquad (3.6)$$

while the coefficient β is given by

$$\beta = \alpha(2\mu + 3\lambda), \qquad (3.7)$$

where α is the thermal expansion coefficient. In terms of Young's modulus E and Poisson ratio ν, there are

$$\mu = \frac{E}{2(1+\nu)}, \quad \lambda = \frac{\nu E}{(1+\nu)(1-2\nu)}. \qquad (3.8)$$

For plane stress assumption λ and β must be replaced respectively by $\lambda^\star$ in (3.5) and $\beta^\star$ in (3.7), where

$$\lambda^\star = \frac{2\mu\lambda}{\lambda + 2\mu} = \frac{\nu E}{1 - \nu^2}, \quad \beta^\star = 2\alpha(\mu + \lambda^\star). \quad (3.9)$$

The space of kinematically admissible displacements is defined as

$$\mathcal{V}(\Omega) := \left\{\phi \in \mathbf{H}^1(\Omega) : \phi_{|\Gamma_u} = 0\right\}, \qquad (3.10)$$

with $\mathbf{H}^1(\Omega) := H^1(\Omega; \mathbb{R}^2)$ and Γ_u is used to denote a part of the boundary $\partial\Omega$ where the displacement u is prescribed.

From these elements, the equilibrium equation (3.2) leads to the following variational problem: Find the displacement field $u \in \mathcal{V}(\Omega)$, such that

$$\int_\Omega \sigma(u) \cdot (\nabla v)^s = \int_\Omega \beta\theta\mathrm{div}(v) \quad \forall v \in \mathcal{V}(\Omega), \quad (3.11)$$

where the scalar function θ is the solution to the following variational problem: Find the temperature field $\theta \in \mathcal{H}(\Omega)$, such that

$$\int_\Omega q(\theta) \cdot \nabla\eta + \int_\Omega b\eta = 0 \quad \forall \eta \in \mathcal{H}_0(\Omega), \qquad (3.12)$$

with b used to denote a heat source in Ω. The heat flux vector field is defined as

$$q(\theta) = -\mathrm{K}\nabla\theta, \qquad (3.13)$$

where K is a second order tensor representing the thermal conductivity of the medium. In the isotropic case, the tensor K can be written as

$$\mathrm{K} = k\mathrm{I}, \qquad (3.14)$$

being k the thermal conductivity coefficient. The set $\mathcal{H}(\Omega)$ and the space $\mathcal{H}_0(\Omega)$ are respectively defined as

$$\mathcal{H}(\Omega) := \left\{\phi \in H^1(\Omega) : \phi_{|\Gamma_\theta} = \overline{\theta}\right\}, \quad (3.15)$$

$$\mathcal{H}_0(\Omega) := \left\{\phi \in H^1(\Omega) : \phi_{|\Gamma_\theta} = 0\right\}, \quad (3.16)$$

with Γ_θ used to denote a part of the boundary $\partial\Omega$ where the temperature θ is prescribed by a given function $\overline{\theta}$.

Let us also introduce two adjoint auxiliary problems in order to simplify further analysis. The mechanical auxiliary problem reads: find the adjoint displacement field $p \in \mathcal{V}(\Omega)$, such that

$$\int_\Omega \sigma(p) \cdot (\nabla v)^s = \int_{\Gamma^\star} e \cdot v \quad \forall v \in \mathcal{V}(\Omega). \qquad (3.17)$$

The thermal auxiliary problem is stated as: find the adjoint temperature field $\varphi \in \mathcal{H}_0(\Omega)$, such that

$$\int_\Omega q(\varphi) \cdot \nabla\eta = \int_\Omega \beta\mathrm{div}(p)\,\eta \quad \forall \eta \in \mathcal{H}_0(\Omega). \quad (3.18)$$

These adjoint problems result from the Lagrangian formalism, where the associated augmented Lagrangian is minimized with respect to the states u and θ.

3.2. Perturbed Problem.

The perturbation to the basic problem is now introduced by considering a pair of piecewise constant functions γ_ε^M and γ_ε^T, which respectively affect the constitutive tensors $\mathbb{C}$ and K in some small subdomain of the initial structure. In particular, the topologically perturbed counterpart of the shape functional is given by

$$j(\varepsilon) = J_\varepsilon(\Omega) = \mathcal{J}_\Omega(u_\varepsilon) := -\int_{\Gamma^\star} e \cdot u_\varepsilon. \qquad (3.19)$$

The vector function u_ε is the solution to the perturbed coupled system, namely: Find the displacement field $u_\varepsilon \in \mathcal{V}(\Omega)$, such that

$$\int_\Omega \sigma_\varepsilon(u_\varepsilon) \cdot (\nabla v)^s = \int_\Omega \beta_\varepsilon \theta_\varepsilon \mathrm{div}(v) \quad \forall v \in \mathcal{V}(\Omega), \qquad (3.20)$$

where

$$\sigma_\varepsilon(u_\varepsilon) := \gamma_\varepsilon^M \mathbb{C}(\nabla u_\varepsilon)^s = \gamma_\varepsilon^M \sigma(u_\varepsilon), \qquad (3.21)$$

with the contrast on the elastic properties defined as

$$\gamma_\varepsilon^M := \begin{cases} 1 & \text{in} \quad \Omega \setminus \overline{B_\varepsilon} \\ \gamma^M & \text{in} \quad B_\varepsilon \end{cases}. \qquad (3.22)$$

Based on the above definition, the perturbed coefficient β_ε in (3.20) takes the form

$$\beta_\varepsilon := \gamma_\varepsilon^M \beta. \qquad (3.23)$$

The scalar function θ_ε solves the following perturbed variational problem: Find the temperature field $\theta_\varepsilon \in \mathcal{H}(\Omega)$, such that

$$\int_\Omega q_\varepsilon(\theta_\varepsilon) \cdot \nabla \eta + \int_\Omega b_\varepsilon \eta = 0 \quad \forall \eta \in \mathcal{H}_0(\Omega), \qquad (3.24)$$

where

$$q_\varepsilon(\theta_\varepsilon) := -\gamma_\varepsilon^T K \nabla \theta_\varepsilon, \quad b_\varepsilon := \gamma_\varepsilon^T b, \qquad (3.25)$$

with the contrast on the thermal properties defined as

$$\gamma_\varepsilon^T := \begin{cases} 1 & \text{in} \quad \Omega \setminus \overline{B_\varepsilon} \\ \gamma^T & \text{in} \quad B_\varepsilon \end{cases}. \qquad (3.26)$$

Finally, the topologically perturbed counterpart of the mechanical adjoint problem (3.17) reads: Find the adjoint displacement field $p_\varepsilon \in \mathcal{V}(\Omega)$, such that

$$\int_\Omega \sigma_\varepsilon(p_\varepsilon) \cdot (\nabla v)^s = \int_{\Gamma^\star} e \cdot v \quad \forall v \in \mathcal{V}(\Omega), \qquad (3.27)$$

while the topologically perturbed counterpart of the thermal adjoint problem (3.18) is given by: Find the adjoint temperature field $\varphi_\varepsilon \in \mathcal{H}_0(\Omega)$, such that

$$\int_\Omega q_\varepsilon(\varphi_\varepsilon) \cdot \nabla \eta = \int_\Omega \beta \mathrm{div}(p) \eta \quad \forall \eta \in \mathcal{H}_0(\Omega). \qquad (3.28)$$

Remark 1. *The arguments concerning the existence of the topological derivative associated with the problem under analysis can be found in Appendix A.*

Remark 2. *Since we are dealing with a topology optimization problem in a fixed domain Ω, the optimal structure is identified by the elastic material, while a very compliant (weak) material is used to mimic voids, both distributed within Ω. Therefore, we consider contrasts in the Young's modulus E (assuming the Poisson ratio ν as constant) and in the thermal conductivity k only, which are respectively given by γ^M and γ^T. In fact, by setting $\gamma^M \to 0$ and $\gamma^T \to 0$, the transmission conditions on $\partial B_\varepsilon(\widehat{x})$ degenerate to homogeneous Neumann boundary conditions in both mechanical (3.20) and thermal (3.24) problems, respectively representing a void and an ideal thermal insulation. The general case is much more involved, so that we left it for future work.*

4. Topological Asymptotic Analysis

Since the problem under consideration is linear, we firstly set $\gamma^M = 1$ and develop the topological asymptotic analysis for $\gamma^T \neq 1$. Next, we set $\gamma^T = 1$ and develop the analysis for $\gamma^M \neq 1$. Finally, the obtained results are superposed, leading to the associated topological derivative for any pair of γ^M and γ^T. Let us start by evaluating the difference between the original and perturbed shape functionals given respectively by (3.1) and (3.19), which leads to

$$\mathcal{J}_\Omega(u_\varepsilon) - \mathcal{J}_\Omega(u) = -\int_{\Gamma^\star} e \cdot (u_\varepsilon - u). \qquad (4.1)$$

4.1. Contrast on the elastic coefficients.

Let us set $\gamma^T = 1$ and develop the analysis for $\gamma^M \neq 1$. In this case we have immediately that $\theta_\varepsilon \equiv \theta$. By taking $v = u_\varepsilon - u$ in (3.27), we obtain the equality

$$\int_\Omega \sigma_\varepsilon(p_\varepsilon) \cdot (\nabla(u_\varepsilon - u))^s = \int_{\Gamma^\star} e \cdot (u_\varepsilon - u). \qquad (4.2)$$

Now, let us set $v = p_\varepsilon$ in (3.11) and (3.20). After evaluating the difference between the obtained results we get

$$\int_\Omega \sigma_\varepsilon(p_\varepsilon) \cdot (\nabla(u_\varepsilon - u))^s =$$
$$\frac{1 - \gamma^M}{\gamma^M} \int_{B_\varepsilon} \sigma_\varepsilon(p_\varepsilon) \cdot (\nabla u)^s - (1 - \gamma^M) \int_{B_\varepsilon} \beta \theta \mathrm{div}(p_\varepsilon). \qquad (4.3)$$

Therefore, after comparing the last two results with (4.1) we have

$$\mathcal{J}_\Omega(u_\varepsilon) - \mathcal{J}_\Omega(u) =$$
$$-\frac{1 - \gamma^M}{\gamma^M} \int_{B_\varepsilon} \sigma_\varepsilon(p_\varepsilon) \cdot (\nabla u)^s + (1 - \gamma^M) \int_{B_\varepsilon} \beta \theta \mathrm{div}(p_\varepsilon). \qquad (4.4)$$

Let us propose an ansätz for p_ε in the form $p_\varepsilon = p + w_\varepsilon + \widetilde{p}_\varepsilon$, which allows us to choose w_ε as a solution to: Find the exterior displacement field $w_\varepsilon \in \mathbf{W}^1(\mathbb{R}^2)/\mathbb{R}$, such that

$$\int_{\mathbb{R}^2} \sigma_\varepsilon(w_\varepsilon) \cdot (\nabla v)^s =$$
$$(1 - \gamma^M)\sigma(p)(\widehat{x}) \cdot \int_{B_\varepsilon} (\nabla v)^s \quad \forall v \in \mathbf{W}^1(\mathbb{R}^2)/\mathbb{R}. \tag{4.5}$$

where the weighted quotient space $\mathbf{W}^1(\mathbb{R}^2)/\mathbb{R}$ has been introduced in (Amstutz et al., 2014, App. C) to ensure existence and uniqueness of a solution to the above exterior problem. From Eshelby's Theorem (Eshelby (1957, 1959)), the exterior problem (4.5) admits an explicit solution, namely

$$\sigma_\varepsilon(w_\varepsilon) = \mathbb{T}\sigma(p)(\widehat{x}) \quad \text{in} \quad B_\varepsilon, \tag{4.6}$$

where $\mathbb{T}$ is a fourth order isotropic tensor written as

$$\mathbb{T} = \gamma^M \frac{1 - \gamma^M}{1 + \gamma^M \alpha_2} \left(\alpha_2 \mathbb{I} + \frac{\alpha_1 - \alpha_2}{2(1 + \gamma^M \alpha_1)} \mathrm{I} \otimes \mathrm{I} \right), \tag{4.7}$$

with the constants α_1 and α_2 given by

$$\alpha_1 = \frac{\mu + \lambda}{\mu}, \quad \alpha_2 = \frac{3\mu + \lambda}{\mu + \lambda}. \tag{4.8}$$

See, for instance, the book (Novotny and Sokołowski, 2013, Ch. 5, pp. 156). From Lemma 6 in Appendix A the remainder $\widetilde{p}_\varepsilon$ has an estimate of the form $\|\widetilde{p}_\varepsilon\|_{\mathbf{H}^1(\Omega)} \approx o(\varepsilon)$. Finally, by taking into account these last results, we have the following expansion for the shape functional

$$\mathcal{J}_\Omega(u_\varepsilon) - \mathcal{J}_\Omega(u) = -\pi\varepsilon^2 \mathbb{P}\sigma(u)(\widehat{x}) \cdot (\nabla p)^s(\widehat{x}) +$$

$$\pi\varepsilon^2 \beta(1 + \alpha_1)\frac{1 - \gamma^M}{1 + \gamma^M \alpha_1}\theta(\widehat{x})\mathrm{div}(p)(\widehat{x}) + o(\varepsilon^2). \tag{4.9}$$

where $\mathbb{P}$ is the Polya-Szëgo polarization tensor given by (Ammari and Kang, 2007)

$$\mathbb{P} = \frac{1 - \gamma^M}{1 + \gamma^M \alpha_2} \left((1 + \alpha_2)\mathbb{I} + \frac{1}{2}(\alpha_1 - \alpha_2)\frac{1 - \gamma^M}{1 + \gamma^M \alpha_1}\mathrm{I} \otimes \mathrm{I} \right). \tag{4.10}$$

4.2. **Contrast on the thermal coefficients.** Let us now set $\gamma^M = 1$ and develop the analysis for $\gamma^T \neq 1$. By taking $v = u_\varepsilon - u$ in (3.27), we obtain

$$\int_\Omega \sigma(p) \cdot (\nabla(u_\varepsilon - u))^s = \int_{\Gamma^\star} e \cdot (u_\varepsilon - u). \tag{4.11}$$

Now, let us set $v = p$ in (3.11) and (3.20). After evaluating the difference between the obtained results we get

$$\int_\Omega \sigma(u_\varepsilon - u) \cdot (\nabla p)^s = \int_\Omega \beta(\theta_\varepsilon - \theta)\mathrm{div}(p). \tag{4.12}$$

Therefore, after comparing the last two results with (4.1) we have

$$\mathcal{J}_\Omega(u_\varepsilon) - \mathcal{J}_\Omega(u) = -\int_\Omega \beta(\theta_\varepsilon - \theta)\mathrm{div}(p). \tag{4.13}$$

By setting $\eta = \theta_\varepsilon - \theta$ in (3.28) we obtain the following equality

$$\int_\Omega q_\varepsilon(\varphi_\varepsilon) \cdot \nabla(\theta_\varepsilon - \theta) = \int_\Omega \beta(\theta_\varepsilon - \theta)\mathrm{div}(p), \tag{4.14}$$

which leads to

$$\mathcal{J}_\Omega(u_\varepsilon) - \mathcal{J}_\Omega(u) = -\int_\Omega q_\varepsilon(\varphi_\varepsilon) \cdot \nabla(\theta_\varepsilon - \theta). \tag{4.15}$$

Now, let us set $\eta = \varphi_\varepsilon$ in (3.12) and (3.24). After evaluating the difference between the obtained results we get

$$\int_\Omega q_\varepsilon(\theta_\varepsilon - \theta) \cdot \nabla\varphi_\varepsilon =$$
$$(1 - \gamma^T) \int_{B_\varepsilon} q(\theta) \cdot \nabla\varphi_\varepsilon + (1 - \gamma^T) \int_{B_\varepsilon} b\varphi_\varepsilon. \tag{4.16}$$

After comparing the last two results with (4.15) we finally obtain

$$\mathcal{J}_\Omega(u_\varepsilon) - \mathcal{J}_\Omega(u) =$$
$$-\frac{1 - \gamma^T}{\gamma^T} \int_{B_\varepsilon} q_\varepsilon(\varphi_\varepsilon) \cdot \nabla\theta - (1 - \gamma^T) \int_{B_\varepsilon} b\varphi_\varepsilon. \tag{4.17}$$

Let us propose an ansätz for φ_ε in the form $\varphi_\varepsilon = \varphi + \vartheta_\varepsilon + \widetilde{\varphi}_\varepsilon$, which allows us to choose ϑ_ε as a solution to: Find the exterior temperature field $\vartheta_\varepsilon \in W^1(\mathbb{R}^2)/\mathbb{R}$, such that

$$\int_{\mathbb{R}^2} q_\varepsilon(\vartheta_\varepsilon) \cdot \nabla\eta =$$
$$(1 - \gamma^T)q(\theta)(\widehat{x}) \cdot \int_{B_\varepsilon} \nabla\eta \quad \forall\eta \in W^1(\mathbb{R}^2)/\mathbb{R}, \tag{4.18}$$

where the weighted quotient space $W^1(\mathbb{R}^2)/\mathbb{R}$ has been introduced in (Amstutz et al., 2014, App. C) to ensure existence and uniqueness of a solution to the above exterior problem. The exterior problem (4.18) admits an explicit solution, namely

$$q_\varepsilon(\vartheta_\varepsilon) = \gamma^T \frac{1 - \gamma^T}{1 + \gamma^T}q(\varphi)(\widehat{x}) \quad \text{in} \quad B_\varepsilon. \tag{4.19}$$

See, for instance, the book (Novotny and Sokołowski, 2013, Ch. 5, pp. 144). From Lemma 7 in Appendix A we have that the remainder $\widetilde{\varphi}_\varepsilon$ has an estimate of the form $\|\widetilde{\varphi}_\varepsilon\|_{H^1(\Omega)} \approx o(\varepsilon)$. From these last results, we have the following expansion for the shape

functional

$$\mathcal{J}_\Omega(u_\varepsilon) - \mathcal{J}_\Omega(u) = -\pi\varepsilon^2 \mathrm{P}q(\theta)(\widehat{x}) \cdot \nabla\varphi(\widehat{x}) -$$
$$\pi\varepsilon^2(1-\gamma^T)b\varphi(\widehat{x}) + o(\varepsilon^2), \quad (4.20)$$

where P is the Polya-Szëgo polarization tensor given by (Ammari and Kang, 2007)

$$\mathrm{P} = 2\frac{1-\gamma^T}{1+\gamma^T}\mathrm{I}. \qquad (4.21)$$

4.3. **Topological Derivative.** Since the problem is linear, we can sum the obtained expansions (4.9) and (4.20) to obtain

$$\mathcal{J}_\Omega(u_\varepsilon) - \mathcal{J}_\Omega(u) = -\pi\varepsilon^2 \mathbb{P}\sigma(u)(\widehat{x}) \cdot (\nabla p)^s(\widehat{x}) +$$
$$\pi\varepsilon^2\beta(1+\alpha_1)\frac{1-\gamma^M}{1+\gamma^M\alpha_1}\theta(\widehat{x})\mathrm{div}(p)(\widehat{x}) -$$
$$\pi\varepsilon^2\mathrm{P}q(\theta)(\widehat{x}) \cdot \nabla\varphi(\widehat{x}) - \pi\varepsilon^2(1-\gamma^T)b\varphi(\widehat{x}) + o(\varepsilon^2),$$
$$(4.22)$$

which ensures the existence for the topological derivative of the shape functional $J(\Omega)$ for $f(\varepsilon) = \pi\varepsilon^2$, provided that the remainder has order $o(\varepsilon^2)$. Finally, the topological derivative can be promptly identified, which is given by the following closed formula

$$\mathcal{T}(\widehat{x}) = -\mathbb{P}\sigma(u)(\widehat{x}) \cdot (\nabla p)^s(\widehat{x})$$
$$+ \beta(1+\alpha_1)\frac{1-\gamma^M}{1+\gamma^M\alpha_1}\theta(\widehat{x})\mathrm{div}(p)(\widehat{x})$$
$$- \mathrm{P}q(\theta)(\widehat{x}) \cdot \nabla\varphi(\widehat{x}) - (1-\gamma^T)b\varphi(\widehat{x}). \quad (4.23)$$

For the reader convenience, we present the above formula in standard index notation, namely

$$\mathcal{T}(\widehat{x}) = -\frac{1}{2}\widetilde{\alpha}_2(1+\alpha_2)\sigma_{ij}(u)(\widehat{x})(\partial_i p_j(\widehat{x}) + \partial_j p_i(\widehat{x}))$$
$$- \frac{1}{2}(\alpha_1 - \alpha_2)\widetilde{\alpha}_1\widetilde{\alpha}_2\sigma_{ii}(u)(\widehat{x})\partial_i p_i(\widehat{x})$$
$$+ \beta(1+\alpha_1)\widetilde{\alpha}_1\theta(\widehat{x})\partial_i p_i(\widehat{x})$$
$$- 2\frac{1-\gamma^T}{1+\gamma^T}q_i(\theta)(\widehat{x})\partial_i\varphi(\widehat{x}) - (1-\gamma^T)b\varphi(\widehat{x}). \quad (4.24)$$

where the coefficients $\widetilde{\alpha}_1$ and $\widetilde{\alpha}_2$ are respectively given by

$$\widetilde{\alpha}_1 = \frac{1-\gamma^M}{1+\gamma^M\alpha_1} \quad \text{and} \quad \widetilde{\alpha}_2 = \frac{1-\gamma^M}{1+\gamma^M\alpha_2} \qquad (4.25)$$

Notice that the closed formula for the topological derivative depends only on the solution of the direct and adjoint problems, given by eqs. (3.11), (3.12), (3.17) and (3.18), evaluated at the point $\widehat{x}$. This derivative represents the sensitivity of the multi-physics problem presented in Section 3 to the insertion of a circular inclusion of radius ε and center at an arbitrary point $\widehat{x} \in \Omega$, whose constitutive properties are characterized by the contrasts γ^M and γ^T.

5. Numerical Experiments

In this section two numerical examples of topology design of thermomechanical actuators into plane stress assumptions are presented. The topology design algorithm developed by Amstutz and Andrä (2006) is adopted in order to solve the optimization problem, which is based on the topological derivative concept together with a level-set domain representation method. For further details of the algorithm we refer to the work by Amstutz and Novotny (2010). In all examples we consider the following constitutive properties: $E = 1\,\mathrm{GPa}$ (Young's modulus), $\nu = 0.3$ (Poisson's ratio), $\alpha = 1.0 \times 10^{-6}\,\mathrm{K}^{-1}$ and $k = 1.0\,\mathrm{W/mK}$. The contrast parameters are given by $\gamma^M = \gamma^T = 1.0 \times 10^{-4}$, which are used to mimic the voids. In the part of the boundary where nothing is specified, we consider homogeneous Neumann boundary conditions in both problems (mechanical and thermal). The direction e is given by a unit vector on $\Gamma^\star$. In addition, we do not consider a heat source, i.e. $b = 0$. The thermomechanical problem (3.11), the steady-state heat conduction problem (3.12) and the adjoint equations (3.17) and (3.18) are solved by using the standard finite element method (Zienkiewicz and Taylor, 2000). The initial mesh is generated from a regular grid of size 20×12, where each resulting square is divided into four triangles, leading to 960 elements. Then, four steps of uniform mesh refinement are performed during the iterative process. In the figures, black and white are respectively used to represent solid and void, whereas the color levels black/brown to yellow/white indicate colder to hotter, respectively. Finally, the procedures described by Campeão et al. (2014) were used to impose a targeted final volume.

Remark 3. *We point out that numerical results obtained in the paper are not directly utilizable in engineering practice. In particular, in practical designs all singularities of solutions to state equations should be removed to avoid e.g., the damage. In addition, it is remarked that a local, mesh-dependent optimal design was found for the problems under consideration.*

5.1. **Example 1: Amplifier.** The first example is the optimization of a displacement amplifier. This device is used to amplify the displacements in a given direction generated by thermal effects. In particular, the design domain considered is presented in Fig. 2, in which only one quadrant of the complete domain is represented, based on horizontal and vertical symmetry assumptions (the dashed-dot lines indicate the

axes of symmetry). The objective is the maximization of the outward output displacement in the direction e on $\Gamma^\star$ in response to a thermal excitation imposed on Γ_θ. In this case, the boundary condition is given by a linear temperature distribution on Γ_θ, as shown in Fig. 2(b). The material properties are optimized in white subdomains, while in the light grey regions of Figs. 2(a) and 2(b) the material properties are fixed.
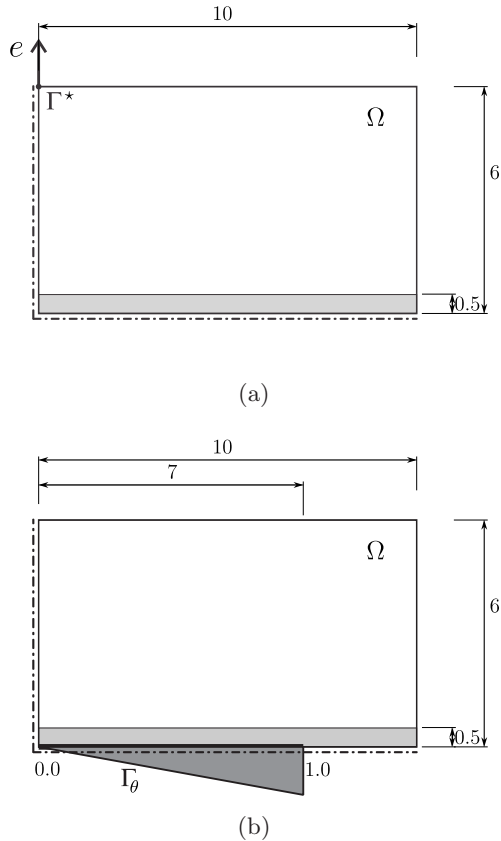

(a)

(b)

FIGURE 2. Example 1. Domain and boundary conditions: (a) mechanical problem and (b) heat problem.

In Fig. 3, the results for two different volume fractions are shown. Also, in Fig. 4 a selected result is shown without the symmetry boundary condition. The amplified deformed configuration of a selected result is shown in Fig. 6(a). In order to analyze the results from a quantitative point of view we define an effectiveness factor $\Lambda := \mathcal{J}_\Omega(u_{ini})/\mathcal{J}_\Omega(u_{opt})$, where u_{ini} and u_{opt} are the displacements of the *initial* and *optimized* configurations, respectively. This effectiveness factor can be viewed as a particularization of the standard *geometric advantage (GA)* metric, used in the design and performance studies of compliance mechanisms. See for instance Howell et al. (2013). The GA measures the relation between the obtained displacement u_{out} when the device is actuated by an input displacement u_{in}, i.e. $GA := u_{out}/u_{in}$. Here, the factor Λ measures the GA with respect to the obtained displacement of the reference (initial) configuration.

The variation of the effectiveness values Λ with respect to the final volume fraction are presented in Fig. 5. From the amplified deformed configurations we noticed that the actuator generates the desired displacement.
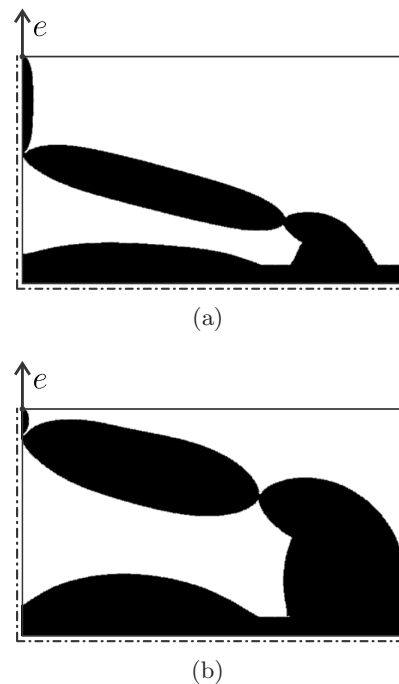

(a)

(b)

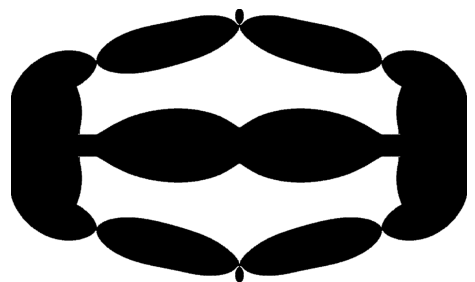FIGURE 3. Example 1. Results for different volume fractions: (a) 30% and (b) 50%.
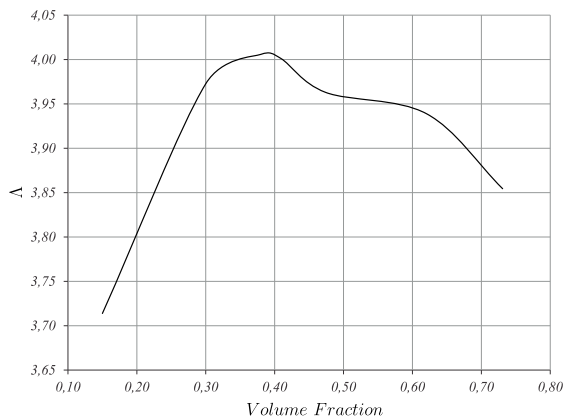

FIGURE 4. Example 1. Amplifier from Fig. 3(b)

FIGURE 5. Example 1. Effectiveness factor vs. final volume fraction.

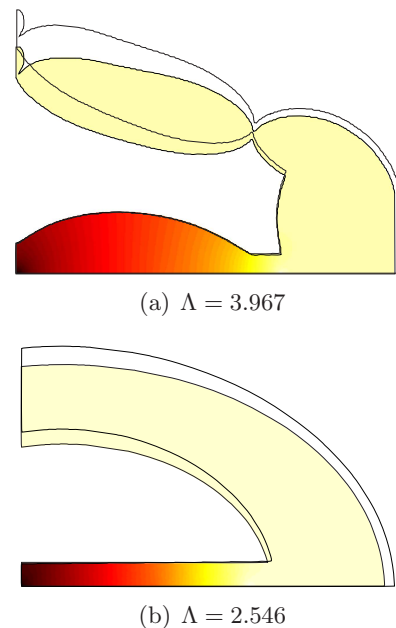(a) $\Lambda = 3.967$

(b) $\Lambda = 2.546$

FIGURE 6. Example 1. Amplified deformed configurations and temperature distributions: (a) *optimal* configuration from Fig. 3(b) and (b) *intuitive solution.*

The behavior of the effectiveness factor with respect to the final volume fraction suggests that there exists a volume fraction close to the 40% where the displacement on $\Gamma^\star$ is maximal in the direction e. This value can be interpreted as an *optimal volume fraction* whose associated effectiveness factor is $\Lambda = 4.01$.

After an inspection of the obtained results, we note the presence of flexible hinges in the design (see Remark 3). These hinges allow for high values of Λ. The hinges generated in optimal design, see Fig.6(a), assure easy rotation of the upper lever elements in order to produce maximal displacement along the symmetry axis. Here, we can refer to the simple example in Section 1.1 illustrating the optimal mode of deformation. However, the hinges are undesirable for obvious reasons. Actually, they can induce large local stress concentration, so in real design the final material segments should be used. Such a pathology is a consequence of the adopted formulation based on compliance maximization. How to avoid these hinges is a subject of recent research and it is out of the scope of this paper (see, for instance, the papers by Lee and Gea (2014) and Lopes and Novotny (2016)). On the other hand, the results previously presented can be interpreted, from an engineering point of view, as a ring connected by a transversal bar. This *intuitive* solution is hinge-free and produces a displacement in the desired direction e, but with an effectiveness factor smaller than the one obtained through the methodology presented in this paper. Actually, in Fig. 6 the amplified deformed configurations of a selected optimal solution and from an *intuitive solution* are presented (we recall that only a quarter of the domain is modeled). Also, the temperature distribution field in both devices are shown together with their associated effectiveness factors Λ.

5.2. **Example 2: Inverter with eccentricity effect.** The second example considers the same domain from the previous experiment, however, the output displacement region $\Gamma^\star$ is changed as depicted in Fig. 7. This apparently simple modification in the design domain actually results in a completely different mechanism, since the optimizer seeks an output displacement contrary to the natural movement of the thermomechanical device. In addition, all symmetry assumptions remain valid and the boundary condition for thermal problem is given by a linear temperature distribution on Γ_θ, as shown in Fig. 7(b). The material properties are optimized in white subdomains, while in the light grey regions of Figs. 7(a) and 7(b) the material properties are fixed, as in the previous example.
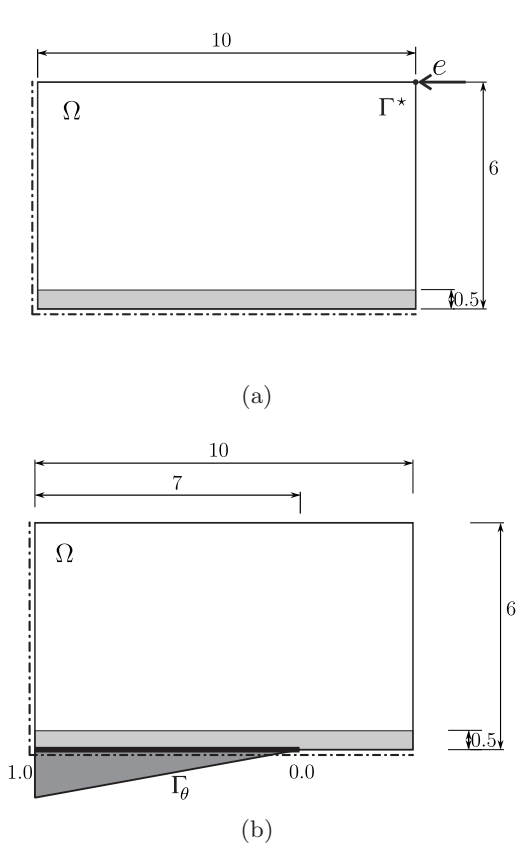
(a)

(b)

FIGURE 7. Example 2. Domain and boundary conditions: (a) mechanical problem and (b) thermal problem.
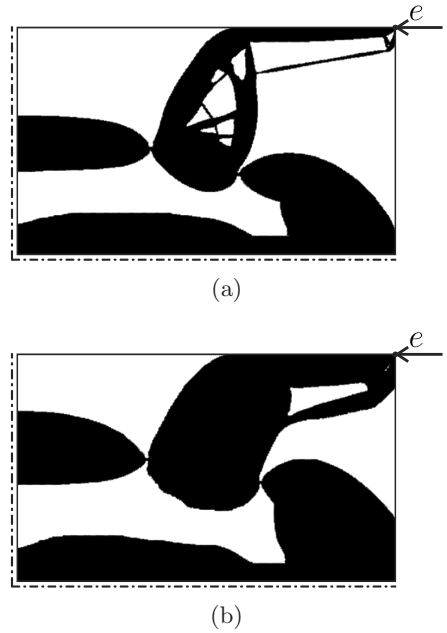

(a)

(b)

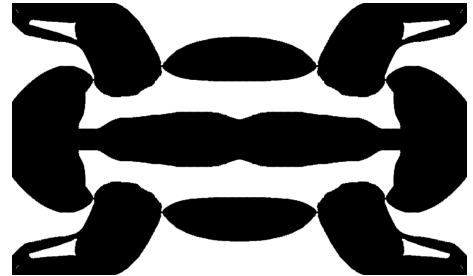FIGURE 8. Example 2. Results for different volume fractions: (a) 45% and (b) 60%.
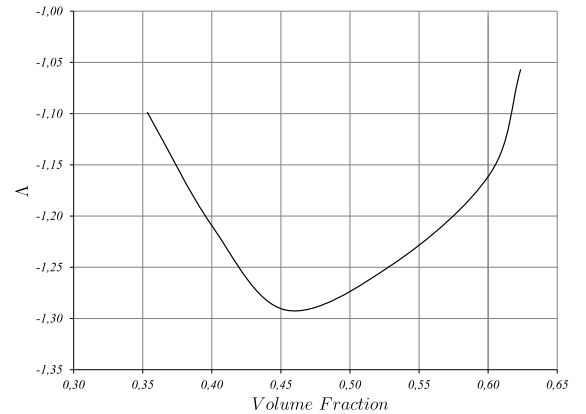

FIGURE 9. Example 2. Inverter from Fig. 8(b)

FIGURE 10. Example 2. Effectiveness factor vs. final volume fraction.

In Fig. 8, the results for two different volume fractions are shown. In Fig. 9 a selected result is shown without the symmetry boundary condition. The amplified deformed configuration of a selected result is shown in Fig. 11(a). Here, also, we notice the presence of flexible hinges in the design (see Remark 3). Referring to Figs. 8 and 9 it is seen that the contact forces at hinge points with upper lever elements induce the rotation moments producing large displacement in the e-direction. The values for the effectiveness factor Λ for the obtained results are presented in Fig. 10, where the negative sign for Λ indicates the inversion of the direction of the displacement (as shown in the amplified deformed configuration Fig. 11(a)). Also, in this example, the effectiveness factor has a minimum value between 45% and 50% of volume fraction. This behavior suggests that there exists a volume fraction where the displacement on $\Gamma^\star$ is maximal in the direction e.
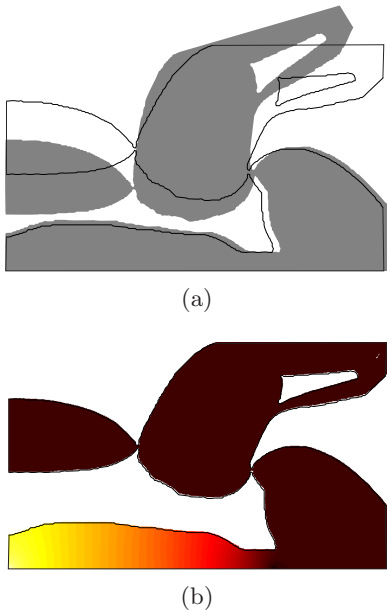
(a)

(b)

FIGURE 11. Example 2. Amplified deformed configuration (a) for result from Fig. 8(b) and temperature distribution (b).

6. CONCLUDING REMARKS

In the paper the topological derivative of the tracking-type shape functional for the semi-coupled thermomechanical model are derived in two spatial dimensions. In order to avoid complicated theoretical derivations such as the ones presented by Giusti et al. (2013), the thermal expansion coefficients have been fixed. By introducing contrasts on the thermal conductivity coefficient and elastic modulus, the derivations become much simpler, allowing us to focus on the main contribution of the paper, namely: a simple and analytical expression of the topological derivative to be used in the design of thermal-mechanical actuators, where the contrasts in the material properties are used just to mimic voids. Actually, the information provided by the topological derivative $\mathcal{T}(\hat{x})$ can be used as a steepest descent direction in an optimal design algorithm. To illustrate this feature, two numerical experiments associated with the topology optimization of actuators have been presented. These simple examples show the applicability of the proposed methodology in the context of optimal design of thermomechanical devices. Furthermore, we have shown that the proposed methodology allows for finding the optimal volume fraction after some realizations. That is, the volume of the actuator which produces the maximal effectiveness factor Λ for a given direction e. Finally, the remarkable simplicity of topological derivative formula

(4.23) has to be noted: once the temperature distribution θ (solution of (3.12)), displacement field u (solution of (3.11)), thermal adjoint state φ (solution of (3.18)) and mechanical adjoint state p (solution of (3.17)) are obtained in the original (unperturbed) domain Ω, the topological derivative $\mathcal{T}(\hat{x})$ can be evaluated at all $\hat{x} \in \Omega$ using standard postprocessing procedures. Therefore the resulting topology design algorithms based on the topological derivative concept are in general very fast and easy to implement.

APPENDIX A. EXISTENCE OF THE TOPOLOGICAL DERIVATIVE

The following results ensure the existence of the topological derivative associated with the problem under analysis.

Lemma 4. *Let θ and θ_ε be solutions to (3.12) and (3.24), respectively. Then we have that the following estimate holds true*

$$\|\theta_\varepsilon - \theta\|_{H^1(\Omega)} \leq C\varepsilon. \qquad (A.1)$$

Proof. We start by subtracting the variational problem (3.12) from (3.24). After some manipulations there is:

$$\int_\Omega q_\varepsilon(\theta_\varepsilon - \theta) \cdot \nabla\eta =$$
$$(1 - \gamma^T) \int_{B_\varepsilon} q(\theta) \cdot \nabla\eta + (1 - \gamma^T) \int_{B_\varepsilon} b\eta, \quad (A.2)$$

where we have used the fact that $q_\varepsilon(\phi) = q(\phi)$ and $b_\varepsilon = b$ in $\Omega \setminus \overline{B_\varepsilon}$, and $q_\varepsilon(\phi) = \gamma^T q(\phi)$ and $b_\varepsilon = \gamma^T b$ in B_ε. By taking $\eta = \theta_\varepsilon - \theta$ as a test function in the above equation we obtain the following equality

$$\int_\Omega q_\varepsilon(\theta_\varepsilon - \theta) \cdot \nabla(\theta_\varepsilon - \theta) =$$
$$(1 - \gamma^T) \int_{B_\varepsilon} q(\theta) \cdot \nabla(\theta_\varepsilon - \theta) +$$
$$(1 - \gamma^T) \int_{B_\varepsilon} b(\theta_\varepsilon - \theta). \quad (A.3)$$

From the Cauchy-Schwartz inequality it follows that

$$\int_\Omega q_\varepsilon(\theta_\varepsilon - \theta) \cdot \nabla(\theta_\varepsilon - \theta) \le$$
$$C_1\|q(\theta)\|_{L^2(B_\varepsilon)}\|\nabla(\theta_\varepsilon - \theta)\|_{L^2(B_\varepsilon)}+$$
$$C_2\|b\|_{L^2(B_\varepsilon)}\|\theta_\varepsilon - \theta\|_{L^2(B_\varepsilon)} \le \varepsilon C_3\|\theta_\varepsilon - \theta\|_{H^1(\Omega)}, \tag{A.4}$$

where we have used the interior elliptic regularity of function θ and the continuity of the function b at the point $\widehat{x} \in \Omega$. Finally, from the coercivity of the bilinear form on the left-hand side of (A.2), namely

$$c\|\theta_\varepsilon - \theta\|^2_{H^1(\Omega)} \le \int_\Omega q_\varepsilon(\theta_\varepsilon - \theta) \cdot \nabla(\theta_\varepsilon - \theta), \tag{A.5}$$

we obtain the result with the constant $C = C_3/c$ independent of the small parameter ε. $\square$

Lemma 5. *Let u and u_ε be solutions to (3.11) and (3.20), respectively. Then we have that the following estimate holds true*

$$\|u_\varepsilon - u\|_{\mathbf{H}^1(\Omega)} \le C\varepsilon. \tag{A.6}$$

Proof. Let us subtract the variational problem (3.11) from (3.20), so that after some manipulations we have:

$$\int_\Omega \sigma_\varepsilon(u_\varepsilon - u) \cdot (\nabla v)^s = \int_\Omega \beta(\theta_\varepsilon - \theta)\mathrm{div}(v)+$$
$$(1 - \gamma^M)\int_{B_\varepsilon}(\sigma(u) + \beta\theta\,\mathrm{I}) \cdot (\nabla v)^s-$$
$$(1 - \gamma^M)\int_{B_\varepsilon}\beta(\theta_\varepsilon - \theta)\mathrm{div}(v), \tag{A.7}$$

where we have used the fact that $\sigma_\varepsilon(\phi) = \sigma(\phi)$ and $\beta_\varepsilon = \beta$ in $\Omega \setminus \overline{B_\varepsilon}$, and $\sigma_\varepsilon(\phi) = \gamma^M\sigma(\phi)$ and $\beta_\varepsilon = \gamma^M\beta$ in B_ε. By taking $v = u_\varepsilon - u$ as test function in the above equation we obtain the following equality

$$\int_\Omega \sigma_\varepsilon(u_\varepsilon - u) \cdot (\nabla(u_\varepsilon - u))^s = \int_\Omega \beta(\theta_\varepsilon - \theta)\mathrm{div}(u_\varepsilon - u)+$$
$$(1 - \gamma^M)\int_{B_\varepsilon}(\sigma(u) + \beta\theta\,\mathrm{I}) \cdot (\nabla(u_\varepsilon - u))^s-$$
$$(1 - \gamma^M)\int_{B_\varepsilon}\beta(\theta_\varepsilon - \theta)\mathrm{div}(u_\varepsilon - u). \tag{A.8}$$

From the Cauchy-Schwartz inequality it follows that

$$\int_\Omega \sigma_\varepsilon(u_\varepsilon - u) \cdot (\nabla(u_\varepsilon - u))^s \le$$
$$C_1\|\theta_\varepsilon - \theta\|_{L^2(\Omega)}\|\nabla(u_\varepsilon - u)\|_{\mathbf{L}^2(\Omega)}+$$
$$C_2\|\sigma(u) + \beta\theta\,\mathrm{I}\|_{\mathbf{L}^2(B_\varepsilon)}\|\nabla(u_\varepsilon - u)\|_{\mathbf{L}^2(B_\varepsilon)}+$$
$$C_3\|\theta_\varepsilon - \theta\|_{L^2(B_\varepsilon)}\|\nabla(u_\varepsilon - u)\|_{\mathbf{L}^2(B_\varepsilon)} \le$$
$$C_4\|\theta_\varepsilon - \theta\|_{H^1(\Omega)}\|u_\varepsilon - u\|_{\mathbf{H}^1(\Omega)} + \varepsilon C_5\|u_\varepsilon - u\|_{\mathbf{H}^1(\Omega)}, \tag{A.9}$$

where we have used the interior elliptic regularity of function u and the continuity of the function β at the point $\widehat{x} \in \Omega$. From Lemma 4 we have now

$$\int_\Omega \sigma_\varepsilon(u_\varepsilon - u) \cdot (\nabla(u_\varepsilon - u))^s \le C_6\varepsilon\|u_\varepsilon - u\|_{\mathbf{H}^1(\Omega)}. \tag{A.10}$$

Finally, from the coercivity of the bilinear form on the left-hand side of (A.7), namely

$$c\|u_\varepsilon - u\|^2_{\mathbf{H}^1(\Omega)} \le \int_\Omega \sigma_\varepsilon(u_\varepsilon - u) \cdot (\nabla(u_\varepsilon - u))^s \tag{A.11}$$

we obtain the result with the constant $C = C_6/c$ independent of the small parameter ε. $\square$

Lemma 6. *Let p and p_ε be solutions to (3.17) and (3.27), respectively. Then we have that the following estimate holds true*

$$\|p_\varepsilon - p\|_{\mathbf{H}^1(\Omega)} \le C\varepsilon. \tag{A.12}$$

Proof. After subtracting the variational problem (3.17) from (3.27) we have:

$$\int_\Omega \sigma_\varepsilon(p_\varepsilon - p) \cdot (\nabla v)^s = (1 - \gamma^M)\int_{B_\varepsilon}\sigma(p) \cdot (\nabla v)^s \tag{A.13}$$

where we have used the fact that $\sigma_\varepsilon(\phi) = \sigma(\phi)$ in $\Omega \setminus \overline{B_\varepsilon}$ and $\sigma_\varepsilon(\phi) = \gamma^M\sigma(\phi)$ in B_ε. By taking $v = p_\varepsilon - p$ as test function in the above equation we obtain the following equality

$$\int_\Omega \sigma_\varepsilon(p_\varepsilon - p) \cdot (\nabla(p_\varepsilon - p))^s =$$
$$(1 - \gamma^M)\int_{B_\varepsilon}\sigma(p) \cdot (\nabla(p_\varepsilon - p))^s. \tag{A.14}$$

From the Cauchy-Schwartz inequality it follows that

$$\int_\Omega \sigma_\varepsilon(p_\varepsilon - p) \cdot (\nabla(p_\varepsilon - p))^s \le$$
$$C_1\|\sigma(p)\|_{\mathbf{L}^2(B_\varepsilon)}\|\nabla(p_\varepsilon - p)\|_{\mathbf{L}^2(B_\varepsilon)} \le \varepsilon C_2\|p_\varepsilon - p\|_{\mathbf{H}^1(\Omega)}, \tag{A.15}$$

where we have used the interior elliptic regularity of function p. Finally, from the coercivity of the bilinear form on the left-hand side of (A.13), namely

$$c\|p_\varepsilon - p\|^2_{\mathbf{H}^1(\Omega)} \le \int_\Omega \sigma_\varepsilon(p_\varepsilon - p) \cdot (\nabla(p_\varepsilon - p))^s \tag{A.16}$$

we obtain the result with the constant $C = C_2/c$ independent of the small parameter ε. $\square$

Lemma 7. *Let φ and φ_ε be solutions to (3.18) and (3.28), respectively. Then we have that the following estimate holds true*

$$\|\varphi_\varepsilon - \varphi\|_{H^1(\Omega)} \le C\varepsilon. \tag{A.17}$$

Proof. After subtracting the variational problem (3.18) from (3.28) there is:

$$\int_\Omega q_\varepsilon(\varphi_\varepsilon - \varphi) \cdot \nabla\eta = (1 - \gamma^T)\int_{B_\varepsilon} q(\varphi)\cdot\nabla\eta, \quad \text{(A.18)}$$

where we have used the fact that $q_\varepsilon(\phi) = q(\phi)$ in $\Omega \setminus \overline{B_\varepsilon}$ and $q_\varepsilon(\phi) = \gamma^T q(\phi)$ in B_ε. By taking $\eta = \varphi_\varepsilon - \varphi$ as test function in the above equation we obtain the following equality

$$\int_\Omega q_\varepsilon(\varphi_\varepsilon - \varphi)\cdot\nabla(\varphi_\varepsilon - \varphi) =$$
$$(1 - \gamma^T)\int_{B_\varepsilon} q(\varphi)\cdot\nabla(\varphi_\varepsilon - \varphi). \quad \text{(A.19)}$$

From the Cauchy-Schwartz inequality it follows that

$$\int_\Omega q_\varepsilon(\varphi_\varepsilon - \varphi)\cdot\nabla(\varphi_\varepsilon - \varphi) \le$$
$$C_1\|q(\varphi)\|_{L^2(B_\varepsilon)}\|\nabla(\varphi_\varepsilon - \varphi)\|_{L^2(B_\varepsilon)} \le \varepsilon C_2\|\varphi_\varepsilon - \varphi\|_{H^1(\Omega)}, \quad \text{(A.20)}$$

where we have used the interior elliptic regularity of function φ. Finally, from the coercivity of the bilinear form on the left-hand side of (A.18), namely

$$c\|\varphi_\varepsilon - \varphi\|^2_{H^1(\Omega)} \le \int_\Omega q_\varepsilon(\varphi_\varepsilon - \varphi)\cdot\nabla(\varphi_\varepsilon - \varphi), \quad \text{(A.21)}$$

we obtain the result with the constant $C = C_2/c$ independent of the small parameter ε. $\square$

References

G. Allaire, F. Jouve, and N. Van Goethem. Damage and fracture evolution in brittle materials by shape optimization methods. *Journal of Computational Physics*, 230(12):5010–5044, 2011.

H. Ammari and H. Kang. *Polarization and moment tensors with applications to inverse problems and effective medium theory*. Applied Mathematical Sciences vol. 162. Springer-Verlag, New York, 2007.

S. Amstutz and H. Andrä. A new algorithm for topology optimization using a level-set method. *Journal of Computational Physics*, 216(2):573–588, 2006.

S. Amstutz and A. A. Novotny. Topological optimization of structures subject to von Mises stress constraints. *Structural and Multidisciplinary Optimization*, 41(3):407–420, 2010.

S. Amstutz, S. M. Giusti, A. A. Novotny, and E. A. de Souza Neto. Topological derivative for multi-scale linear elasticity models applied to the synthesis of microstructures. *International Journal for Numerical Methods in Engineering*, 84:733–756, 2010.

S. Amstutz, A. A. Novotny, and N. Van Goethem. Topological sensitivity analysis for elliptic differential operators of order $2m$. *Journal of Differential Equations*, 256:1735–1770, 2014.

D. E. Campeão, S. M. Giusti, and A. A. Novotny. Topology design of plates consedering different volume control methods. *Engineering Computations*, 31(5):826–842, 2014.

J. D. Eshelby. The determination of the elastic field of an ellipsoidal inclusion, and related problems. *Proceedings of the Royal Society: Section A*, 241:376–396, 1957.

J. D. Eshelby. The elastic field outside an ellipsoidal inclusion, and related problems. *Proceedings of the Royal Society: Section A*, 252:561–569, 1959.

S. M. Giusti, A. A. Novotny, J. E. Muñoz Rivera, and J. E. Esparta Rodriguez. Strain energy change to the insertion of inclusions associated to a thermo-mechanical semi-coupled system. *International Journal of Solids and Structures*, 50(9):1303–1313, 2013.

M. Hintermüller and A. Laurain. Multiphase image segmentation and modulation recovery based on shape and topological sensitivity. *Journal of Mathematical Imaging and Vision*, 35:1–22, 2009.

M. Hintermüller, A. Laurain, and A. A. Novotny. Second-order topological expansion for electrical impedance tomography. *Advances in Computational Mathematics*, 36(2):235–265, 2012.

L. L. Howell, S. P. Magleby, and B. M. Olsen. *Handbook of Compliant Mechanisms*. Wiley, Chichester, UK, 2013.

N. Kikuchi, S. Nishiwaki, J. S. O. Fonseca, and E. C. N. Silva. Design optimization method for compliant mechanisms and material microstructure. *Computer Methods in Applied Mechanics and Engineering*, 151(3-4):401–417, 1998.

E. Lee and H. C. Gea. A strain based topology optimization method for compliant mechanism design. *Structure and Multidisciplinary Optmization*, 49:199–207, 2014.

Y. Li, K. Saitou, and N. Kikuchi. Topology optimization of thermally actuated compliant mechanisms considering time-transient effect. *Finite Elements in Analysis and Design*, 40:1317–1331, 2004.

C. G. Lopes and A. A. Novotny. Topology design of compliant mechanisms with stress constraints based on the topological derivative concept. *Structural and Multidisciplinary Optimization (to appear)*, 2016.

Z. Mróz and D. Bojczuk. Shape and topology sensitivity analysis and its application to structural design. *Archive of Applied Mechanics*, 82:1541–1555,

2012.

A. A. Novotny and J. Sokołowski. *Topological derivatives in shape optimization*. Interaction of Mechanics and Mathematics. Springer-Verlag, Berlin, Heidelberg, 2013.

W. M. Rubio, E. C. N. Silva, and S. Nishiwaki. Design of compliant mechanisms considering thermal effect compensation and topology optimization. *Finite Elements in Analysis and Design*, 46:1049–1060, 2010.

O. Sigmund. On the design of compliant mechanisms using topology optimization. *Mechanics of Structures and Machines: An International Journal*, 25 (4):493–524, 1997.

J. Sokołowski and A. Żochowski. On the topological derivative in shape optimization. *SIAM Journal on Control and Optimization*, 37(4):1251–1272, 1999.

J. Sokołowski and J. P. Zolésio. *Introduction to shape optimization - shape sensitivity analysis*. Springer-Verlag, Berlin, Germany, 1992.

N. Van Goethem and A. A. Novotny. Crack nucleation sensitivity analysis. *Mathematical Methods in the Applied Sciences*, 33(16):197–1994, 2010.

O. C. Zienkiewicz and R. L. Taylor. *The Finite Element Method*. Butterworth-Heinemann, Oxford, 5 edition, 2000.

A. Żochowski. Optimal perforation design in 2-dimensional elasticity. *Mechanics of Structures and Machines*, 16(1):17–33, 1988.

(S.M. Giusti) Universidad Tecnológica Nacional, Facultad Regional Córdoba UNT/FRC - CONICET, Maestro M. López esq. Cruz Roja Argentina, X5016ZAA - Córdoba, Argentina.
E-mail address: sgiusti@frc.utn.edu.ar

(Z. Mróz) Institute of Fundamental Technological Research, 5A Pawińskiego St., 00-049 Warsaw, Poland
E-mail address: zmroz@ippt.gov.pl

(A.A. Novotny) Laboratório Nacional de Computação Científica LNCC/MCT, Av. Getúlio Vargas 333, 25651-075 Petrópolis - RJ, Brasil.
E-mail address: novotny@lncc.br

(J. Sokołowski) Université de Lorraine, CNRS, INRIA, Institute Élie Cartan Nancy, UMR7502, BP 239 - 54506 Vandoeuvre Lès Nancy Cedex, France
E-mail address: Jan.Sokolowski@univ-lorraine.fr